1 Datasets

[Training and validating a deep learning system requires data, which can be categorized in two distinct groups. The first group is the data known by the system, which is used during training to increase or validate model performance. Additional to the data used during training is external data, which is needed to validate the generalizability of the model. I.e., how well does the model perform with unknown data, which is assumed to be drawn from the same distribution as the data used during training. It is standard practice to arbitrarily split by a given fraction into the three datasets (training, validation, testing), as outlined above. However, due to the variable seasonal dependency of meteorological data, a naive split of the data could result in seasonally unbalanced datasets. As such, the datasets constructed for this thesis's purpose cover at least a full year. Thus, no dataset is assumed to be skewed in the direction of any season.]

> Dette passer bedre inn i en train-test-split **model development**

To facilitate the development and verification of a high resolution short-term deep learning sea ice forecasting system, several datasets from observations and physical model forecasting systems have been chosen. When selecting appropriate datasets, their spatial resolution as well as release frequency has been considered. Even though several observational sea ice concentration products which cover the region of interest exists, a lot of the satellite products based on passive microwave retrievals are of a too coarse resolution (e.g. Lavergne et al. (2019a) or Kern et al. (2019)) to be able to aid in short term decision making (Wagner et al., 2020). Moreover Synthetic Aperture Radar (SAR) observations such as Sentinel 1A Interferometric Wide swath ($5m \times 20m$) or Extra-Wide swath ($20m \times 40m$) are on a sea ice structure resolving spatial resolution. However the daily SAR coverage is sparse in the Arctic (See Supporting Figure 21) and there are currently no sea ice concentration product based on retrieval algorithms of SAR observations which are known to the author.

Moreover, forecasts can be used as predictors for the deep learning system since they provide information regarding how the conditions should evolve in the period after the forecast has been initialized. Thus giving the deep learning system insight into the future state of the domain while still facilitating operational usage by not relying on e.g. future observations. Hence, atmospheric variables from a regional numerical weather prediction system will be included as input to the model. These variables (wind and temperature) have been chosen due to their physical impact on sea ice, and is assumed to encode information about the future state of sea ice concentration when seen in combination with past and present sea ice concentration by the deep learning system.

Finally, the highest resolution product with an appropriate temporal frequency available are the sea ice charts produced by the NIS (Dinessen et al., 2020). Moreover, the sea ice charts represents an interpretation of different sea ice observations delivered as a product directed towards operational users. Thus, the sea ice charts will serve as the ground truth

Table 1: List of the products used and their applications. The dashed line separates observational products (above) from forecast products (below)

Product	Variables	Training	Verification
Ice charts	SIC	Yes	Yes
OSI-SAF SSMIS	SIC trend	Yes	Yes
OSI-SAF CDR	Ice edge length	No	Yes
AMSR2	SIC	No	Yes
AROME-Arctic	T2M, X-wind, Y-wind	Yes	No
NeXtSIM	SIC	No	Yes
Barents-2.5	SIC	No	Yes

for the model. Furthermore, as a deep learning system can increase its skill by combining correlated variables as input, this thesis will explore the impact caused by including several datasets covering both current observations, past trends as well as forecasted variables on different spatial resolutions as input predictors.

The following section will describe the domain covered for this thesis, followed by a run-down of the satellite products as well as physical models used. Table 1 presents the different products used for this thesis, and whether the product is used to train or verify the model.

1.1 Region of interest

The domain covered by the deep learning system, covers part of the European Arctic, with Svalbard off-centered. The coast of Northern-Norway is located on the Southern Border, the archipelago of Novaya Zemlya on the eastern border with Franz Josef Land located to its north. The northern border reaches (88°N, 79°E). The region is an intersection between the domain covered by the Ice Charts (Dinessen et al., 2020) and AROME Arctic (Müller et al., 2017) as shown in Figure (1). The study area is a commercially active region, with regards to fishing, tourism and shipping (Wagner et al., 2020). Moreover, the sea ice area and extent in the domain have a strong seasonal variability (Cavalieri and Parkinson, 2012).

The domain has a 1km spatial resolution, and contains 1972×1972 equidistant grid points. Compared to the AROME Arctic grid, the model domain has a reduced southern and eastern extent, which is manually subsectioned to conform to the square grid imposed by the U-Net architecture (Ronneberger et al., 2015). Another reason for the reduced
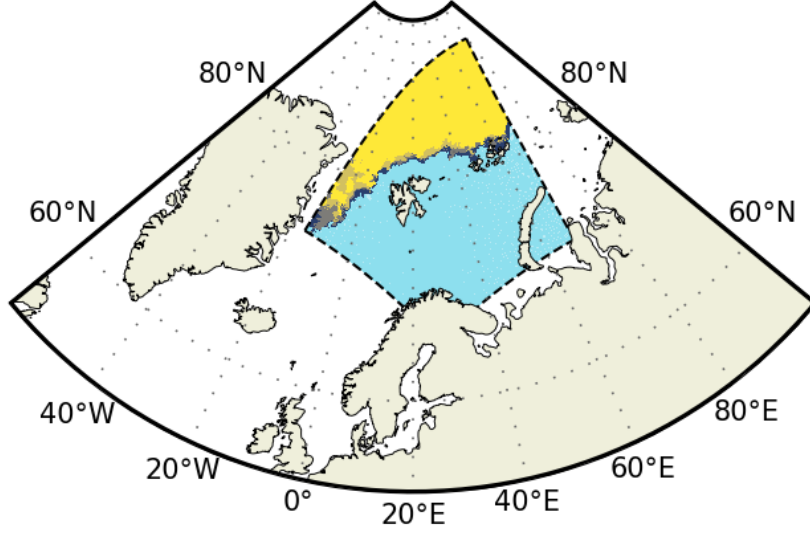
Figure 1: The model domain is shown by sea ice concentration contours retrieved from a sea ice chart (15 Sep 2022). No colorbar is shown, light blue is free open water and yellow is fast ice.

domain extent was to limit the amount of memory needed when loading data during training. Both reasons will be thoroughly discussed in later sections. Moreover, the choice of limiting the southern and eastern extent of the domain was deliberate to reduce the amount of likely sea ice concentration containing grid cells lost in the process.

1.2 Observations

Observations are used to convey the current state of sea ice concentration. There is a lack of consistent in situ observations of sea ice concentration, due to the remoteness of the region. Thus, most independent observations are ship-based concentration estimates (Kern et al., 2019) or optical remote sensing, the latter is only available during summer. As a result, sea ice concentration is mainly observed automatically through passive microwave retrievals utilizing different sea ice retrieval algorithms (Lavergne et al., 2019b; Comiso et al., 1997; Spreen et al., 2008). Another source of sea ice observations are sea ice charts (https://usicecenter.gov/, Last Accessed 25 Jan 2023) (Dinessen et al., 2020), which are manually drawn interpretations combining available sea ice concentration observations such as SAR, passive microwave and optical imagery.

1.2.1 Sea Ice Charts

The sea ice charts utilized for this thesis are provided by the Norwegian Meteorological Institute through the National Ice Service. The product is manually drawn by a sea ice specialist, and is distributed every workday at 15:00 UTC. The Sea Ice specialist assesses available SAR data from Sentinel 1 and Radarsat 2. However, due to the spatial variability in daily SAR coverage (See Supporting Figure (21)), visual, infrared and low resolution passive microwave observations are supplied to achieve a consistent spatial coverage (Dinessen et al., 2020). The sea ice charts are not drawn onto any resolution. Hence, a gridded representation of the ice charts is only a representation of the mean value of the polygons contained inside each grid cell. The sea ice charts used in this work has been interpolated onto a 1-km grid with the same projection as AROME Arctic (Müller et al., 2017).

With regards to consistency, it is noted that the current sea ice chart product have no easily identifiable way of noting which observations were used by the sea ice analyst to draw each segment of the chart. As the different satellite products used have different spatial scales, from meters to kilometers (Dinessen et al., 2020), the underlying uncertainty and ability to resolve structures varies both spatially and temporally. The published sea ice charts as seen in Figure (2) shows the available SAR coverage as black contours, which is the preferred data source for the ice analysts (Dinessen et al., 2020).

Figure (3) shows the monthly distribution of sea ice concentration contours from the sea ice charts during the period of 2022. As can be seen from the figure, more than half of the region consists of ice free open water, with the other majority of an ice chart consisting of very close drift ice. Moreover, the figure shows the seasonal variability of the sea ice extent, with the ice free open water contributing between $\sim 38\%$ and $\sim 75\%$ of the entire domain depending on the month. The ice charts also resolve the intermediate sea ice concentration classes, which for the current region is mostly related to the marginal ice zone and the ice edge.

By inspecting Figure (4), it can be seen that the autocorrelation between two ice charts close in time is high. However, it can also be seen to steadily decline as the time lag increases. From the strong autocorrelation seen in Figure (4), it can be assumed that the persistence for short lead times (days) closely relate to the current sea ice concentration. Furthermore, the autocorrelation also renders previous sea ice concentration at short timescales as skillful at describing the current growth of the sea ice. The latter will be used as motivation to compute a sea ice concentration trend in a coming subsection.

The Sea Ice chart is an operational product mainly targeted for maritime operators. A single sea ice chart is usually drawn by one individual person from the NIS team. However, there are several sea ice specialists at the NIS whom draw ice charts. On the one hand, the
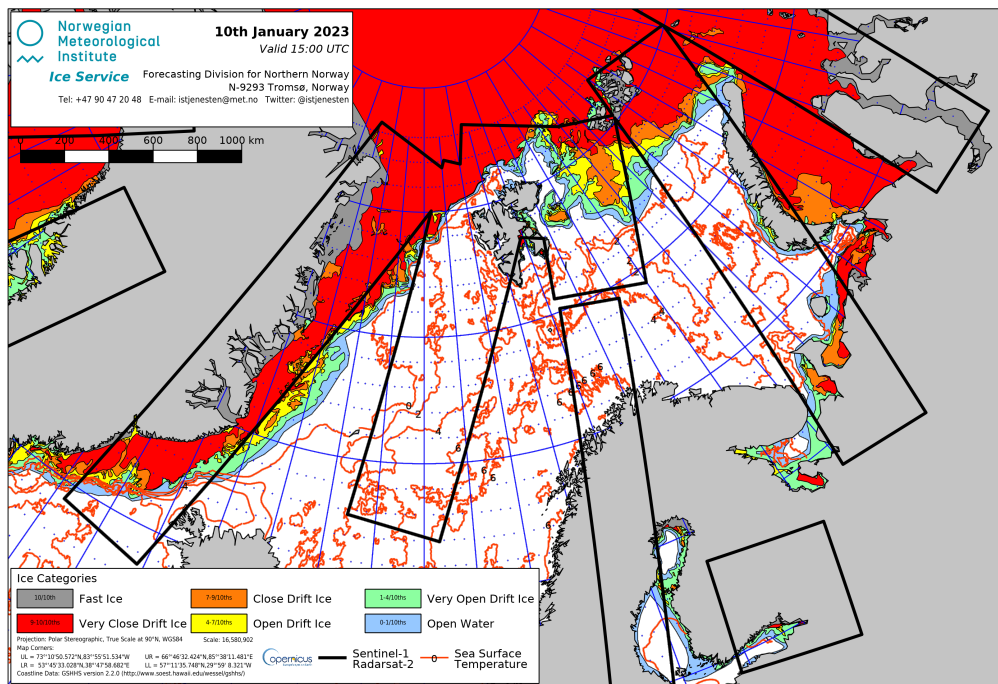
4

Figure 2: Sea Ice chart produced by the NIS covering 10 Jan 2023 at 15:00 UTC. Sea ice concentration categories are drawn as filled contours. The black lines indicate the available SAR data used to draw the sea ice chart.
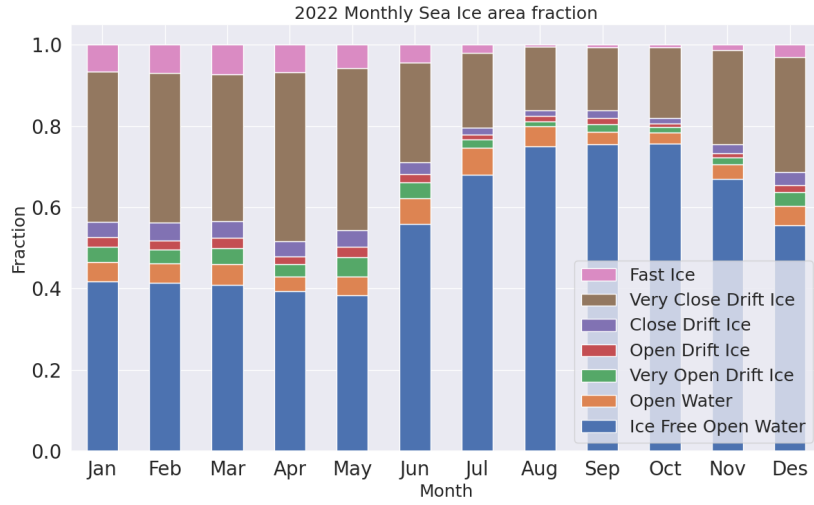
Figure 3: Monthly distribution of each concentration class as respective fraction of the total mean sea ice concentration for the sea ice charts covering 2022. [**Could extend to cover larger time period (e.g. from 2011), give a more climate perspective of the sea ice evolution**], **Add concentration ranges for each class**
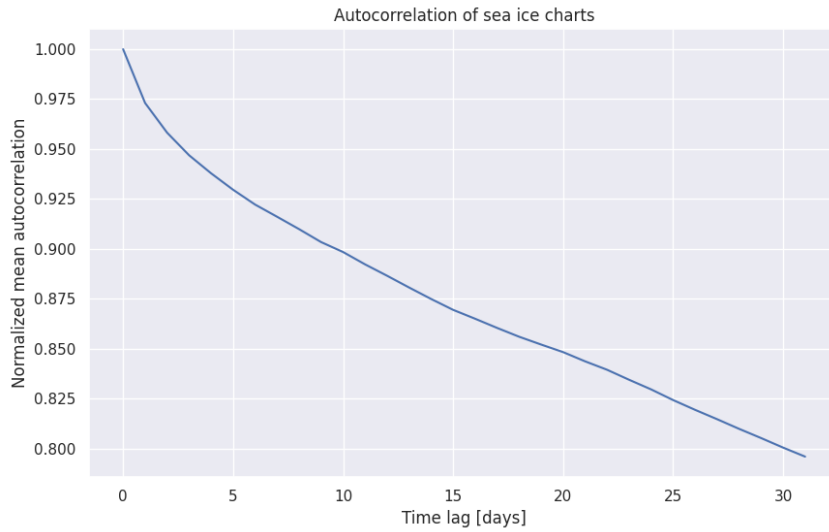

Figure 4: Autocorrelation of the sea ice charts from 2022. The x-axis is the time lag between to entries 2022 sea ice chart timeseries. The y-axis is the normalized autocorrelation, i.e. autocorrelation at a certain time lag divided by the autocorrelation at time lag 0. The autocorrelation is computed for a period covering 31 days.

6

operational nature of the product may influence the decision-making when creating the sea ice charts. Moreover, as a consequence of the human interaction with the production of the sea ice charts it can be assumed that there is an unknown degree of personal bias added to the data. On the other hand, the human involvement may also introduce a degree of quality control not seen in automatic sea ice concentration retrieval algorithms. Thus, the ice charts are assumed to have a low uncertainty, though there are no uncertainty estimates included (Dinessen et al., 2020).

In spite of the uncertainties outlined above, the sea ice charts are assumed to be the most accurate sea ice concentration product available for the purpose of high resolution data tailored towards operational end users. By utilizing the sea ice charts as the ground truth data when training the deep learning system, the developed model will fit towards the proposed high resolution operational use case.

1.2.2 OSI SAF

Two different sea-ice Concentration products are used from OSI SAF. OSI SAF Special Sensor Microwave Imager and Sounder (SSMIS) is an operational product delivering daily sea ice concentration on the northern (and southern) hemisphere. OSI SAF Climate Data Record (CDR) (Sørensen et al., 2021) delivers sea ice concentration beginning in 1979 (Lavergne et al., 2019a). The operational product will be used as a predictor for the model and for validation, whereas the CDR will be used only for validation purposes.

OSI SAF SSMIS

OSI SAF SSMIS is a passive microwave product derived from the (SSMIS) instrument. To convert brightness temperature to estimated sea ice concentration, a hybrid approach combining the Bootstrap algorithm (Comiso et al., 1997) and the Bristol algorithm (Smith, 1996) where the prior is used over open water and the latter used for ice concentrations above 40% (Tonboe et al., 2017). The algorithm uses data from the 19GHz frequency channel (Vertically polarized) and 37GHz channel (Vertically and Horizontally polarized), which are the two lowest spectral resolution channels for the SSMIS Tonboe et al. (2017). Finally, atmospheric corrections are made using analyses from the European Center for Medium Range Weather Forecasts (ECMWF). The end product is delivered every day on a 10km polar stereographic grid.

With regards to uncertainty, OSI SAF SSMIS is validated against pan-arctic sea ice charts from the U.S. National Ice Center as well as regional sea ice charts covering the Svalbard region from the NIS. Moreover, the operational product is required to have a bias and standard deviation less then 10% ice concentration on an annual basis, when compared to the targets (https://osisaf-hl.met.no/sea-ice-conc-edge-validation, Last Accessed 24 Jan 2023) (Lavelle et al., 2017). This strengthens the assumption made at the

end of Section (1.2.1) regarding the accuracy of the sea ice charts and their validity in terms of serving as an independent source for reference.

The operational OSI SAF SSMIS dataset is used to compute a coarse resolution (with respect to the ice charts) linear sea ice concentration trend in each grid cell, with a short term length covering a given amount of days backwards in time. The idea behind the computed trend is to encode multiple time-steps of sea ice concentration fields into a single 2d-array, in line with the lack of temporal awareness of the U-Net architecture. Moreover, the trend serve to limit the size of the training data, since the memory needed is equal to that of a single 2d-array regardless of the length of the trend. Furthermore, the ice concentration trend is computed from a separate sea ice product than the ice chart, with the intent to supply the model with correlated but not overlapping information, as the current day ice chart is already used as a predictor. However, it should also be noted that the lack of sea ice charts during the weekends (Dinessen et al., 2020) is also a contributing factor. As a sea ice concentration trend derived from Dinessen et al. (2020) would be limited to at most five days, which is not the case for OSI SAF SSMIS as there are no temporal gaps in the dataset. The coarser resolution also contributes to the OSI SAF trend serving as complementary information to the ice charts, as the coarse resolution makes the trend less resolvent of the local variability which is seen in the ice charts. As such, the trend serves as a indicator of where the sea ice growth / decline is occurring.

The temporal length used when deriving the trend will have an impact on how the trend reflects the current growth and decline zones, especially with regards to the volatile position of the ice edge on a daily timescale but also due to the seasonal variability of the ice area (Holland and Kimura, 2016). Hence, a too large lookbehind would cause a decorrelation between the current sea ice concentration and the computed trend. Nevertheless, Figure (4) shows that there is significant autocorrelation for sea ice concentration on a short time-range, as described previously. However, a trend computed from a sufficiently long temporal window could be assumed to better represent the spatial distribution of seasonal sea ice concentration growth and decline rather than representing the current growth and decline.

OSI SAF Climate Data Record

As briefly mentioned in Section (1), OSI SAF Climate Data record combines observations from different sensors (SMMR, SSM/I, SSMIS) as well as numerical weather prediction fields from the ERA Interim reanalysis (Dee et al., 2011). The latter are utilized to correct for the atmospheric conditions. Two versions of the dataset has been used, version 2 (OSI-450) which covers (2011 - 2015), and the interim version (OSI-430-b) which cover (2016 - 2020) (https://osisaf-hl.met.no/osi-450-430-b-desc)(Last Accessed 18 Jan 2023). Both products are processed using the same algorithms, ensuring consistency
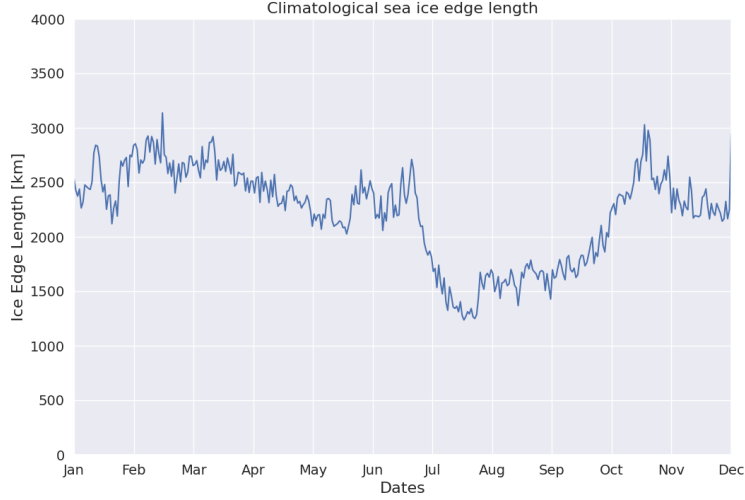
Figure 5: **FIX NONSENSICAL XTICKLABELS** Seasonal variability of the climatological ice edge length computed from satellite observations during the period 2011 - 2020. Only the part of the field projected onto the region of interest has been considered.

(Lavergne et al., 2019b). The Interim version is serving as an extension of the original scope of OSI-450 (1979 - 2015), with a difference being its use of ECMWF analyses compared to the reanalysis and different SSMIS input data (https://osisaf-hl.met.no/osi-450-430-b-desc, Last Accessed 24 Jan 2023). Regardless, both products will hereby be referred to in tandem as OSI SAF CDR

The OSI SAF retrieval algorithm has been shown to have strong correlation against ship based measurements (Kern et al., 2019) as well as optical satellite observations during the summer (Kern et al., 2020). Hence, OSI SAF CDR is expected to serve as a low error representation of the Arctic sea ice concentration. However it is noted that no retrieval algorithm is able to match the true state of the sea ice concentration.

OSI SAF CDR is provided with a 25km spatial resolution on a Lambert Azimuthal Grid projection (Sørensen et al., 2021). The sea ice concentration data retrieved has been used to compute a climatological ice edge length for each day of the year, applying a daily mean across the time period (2011 - 2020). The ice edge length has been computed according to Melsom et al. (2019), which will be derived in Section (1.6.1). Note that though OSI SAF CDR provides a pan-arctic distribution of sea ice concentration, the data has been regridded onto the study region domain with the AROME Arctic projection and a 25km grid spacing before computing the ice edge length.

As can be seen in Figure (5), the Arctic sea ice edge experiences a strong seasonal vari-

ability. The computed climatological ice edge will be used as a normalization factor in order to use verification scores that are not seasonally dependent (Goessling et al., 2016; Zampieri et al., 2019; Palerme et al., 2019). Another benefit from utilizing a single ice edge length is to ensure that different sea ice products are normalized according to a common and independent sea ice length. Furthermore, it will be shown in a later section that the Integrated Ice Edge Error (Goessling et al., 2016) (1.6.2) normalized by the ice edge length is correlated with the resolution of the ice edge length, proving the validity of normalizing using a common, coarse resolution ice edge length.

1.2.3 AMSR2

The Advanced Microwave Scanning Radiometer 2 (AMSR2) data utilized for this thesis is the sea ice concentration product from the University of Bremen (https://seaice.uni-bremen.de/sea-ice-concentration/amsre-amsr2/)(Last Accessed 18 Jan 2023) (Spreen et al., 2008). AMSR2 is a passive microwave sensor observing the microwaves emitted by the Earth, similar to **OSI SAF SSMIS**. AMSR2 is located on the JAXA GCOM-W1 satellite Melsheimer (2019), and the sea-ice concentration is retrieved using the ASI algorithm Spreen et al. (2008). The algorithm uses data from the 89GHz channel, which is the band with the highest spectral resolution, in both polarizations to determine the sea ice concentration. Bands at lower spectral resolutions are only used as weather filters, which can mask out false sea ice detected in the open ocean Spreen et al. (2008). The resulting data is a pan-arctic sea ice coverage with a spatial resolution of 6.25km.

The current AMSR2 product was chosen as the ASI retrieval algorithm (Spreen et al., 2008) results in a higher spatial resolution product compared to similar AMSR2 products such as the AMSR2 product from OSI SAF (Lavelle et al., 2016), which is delivered on a 10km spatial resolution.

Figure (6) shows the monthly distribution of sea ice contours for the AMSR2 dataset. Similarly to Figure (3), a majority of the scenes are covered by Ice Free Open Water. However, Figure (6) shows the AMSR2 dataset has less very close drift ice, which may stem from an increased fast ice contour. Furthermore, AMSR2 has a less resolved open water contour compared to the sea-ice charts. This may be a result of AMSR2 being a algorithmically derived product, whereas the sea-ice charts are drawn for operational use such that regions of potential sea ice encounters are exaggerated to ensure maritime safety. Lastly, Spreen et al. (2008) demonstrated that the ASI algorithm provide the most certainty at concentrations above 65%, with lower concentrations having higher deviations, mainly due to the error contributed by the atmosphere.

As the sea ice charts are treated as the ground truth during training of the deep learning model, it can be assumed that the model is best at predicting sea ice concentration

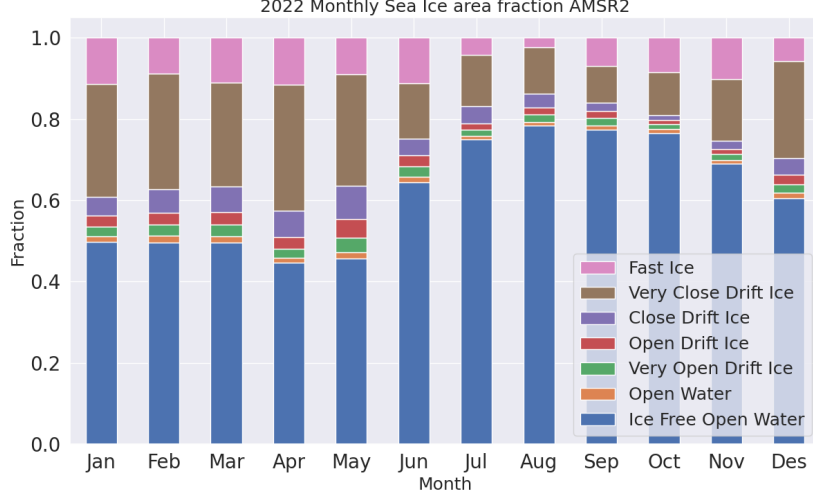DETTE MÅ NEVNES I DISKUSJON NÅR MAN SAM-MEN-LIKNER MOT AMSR2

Figure 6: Monthly distribution of each sea ice concentration class fraction for the AMSR2 dataset covering 2022. The data has been projected onto the region of interest.

distributions similar to those found in the training data. As such, the AMSR2 data will serve as an independent dataset, and will be used for validation only. Thus, the performance of the deep learning system can be inspected with regards to another dataset that is less similar than the sea ice charts, which measures the generalizability of the model.

1.3 Forecasting systems

1.3.1 AROME Arctic

AROME Arctic is a non-hydrostatic, convection resolving high-resolution weather forecasting system which covers the European Arctic (Müller et al., 2017). The model covers the European Arctic similarly to Figure (1) which is the same domain though reduced, with a spatial resolution of 2.5km and 65 vertical levels. AROME Arctic uses different data assimilation techniques for the atmosphere and surface variables. 3DVAR combines the atmospheric model background with observations and is forced by the deterministic ECMWF forecast, whereas optimal interpolation combines the surface model background with observations. Both parts of the data assimilation system is merged to produced the forecast analysis (Müller et al., 2017). As previously mentioned, variables influencing the sea ice concentration can aid in improving the predictive capabilities of a deep learning system. While observational products described above such as the ice charts (Dinessen

et al., 2020) and OSI SAF SSMIS (Tonboe et al., 2017) describe the condition and dynamics of the sea ice concentration. Integrating weather forecast data as part of the model input can be used to describe the interaction between sea ice and atmospheric variables, thus providing relevant variables for predicting sea ice concentration. For the scope of this thesis, 2-meter temperature as well as 10-meter wind in the X and Y component have been selected.

Near surface winds influence the sea ice drift, with the sea ice in the European Arctic displaying a moderate to strong correlation between the sea ice drift speed and the wind speed during winter (Spreen et al., 2011). Moreover, sea ice drift speed is shown to be inversely proportional to the sea ice concentration (Yu et al., 2020). i.e. low concentration sea ice classes tend to have a higher drift speed than high concentration sea ice classes, though both classes display an increased drift speed given an increased near surface wind speed. Thus, including the X and Y component of the near surface wind from AROME Arctic provides the deep learning system with a high resolution proxy for the predicted sea ice drift.

Similarly, surface temperature influences the sea ice mass balance by melting or facilitating sea ice growth (Hibler, 1979), for example through the formation of melt ponds on top of the sea ice. The 2-meter temperature from AROME Arctic is intended to serve as a proxy for the sea ice growth, by including a spatial distribution of temperature to the model. This may be correlated to areas in the model domain experiencing mean positive (melt) or negative (growth) temperatures during the forecast period.

AROME Arctic is shown to have lower RMSE in both 2-meter temperature and 10-meter zonal wind speed than both the deterministic (HRES) and ensemble (ENS) forecast as well as ERA-Interim from ECMWF, for all months when compared to measurements from 89 stations located in Finnmark, Svalbard as well as Jan Mayen and Bjørnøya (Müller et al., 2017). Hence, it is reasonable to assume that extracting the wind and temperature fields from AROME Arctic will provide the most precise information with regards to the strength and spatial location, compared to global medium range numerical weather prediction systems such as the ECMWF Integrated Forecasting System (IFS) Cycle 47r3 (Haiden et al., 2022). However, it is noted that operational numerical weather prediction systems such as those described by Müller et al. (2017) and Haiden et al. (2022) are in constant development, with new improvements added without any retroactive effect for previous data. Firstly, the comparison made in Müller et al. (2017) was with HRES and ENS as of Cycle 38r2 Bauer et al. (2013) is not necessarily representative of the current state of both products. Secondly, significant advances in model development may cause data before and after the implementation date to be inconsistent, e.g. by introducing a permanent shift in bias for a variable. Problems regarding model updates could be avoided by using variables from a re-forecast or reanalysis product such as CARRA (Køltzow et al., 2022). However, CARRA similarly to other

reanalysis products is produced in delayed-mode (see https://climate.copernicus.eu/copernicus-arctic-regional-reanalysis-service, Last Accessed 21 Jan 2023), which would inhibit the operational aspect of the developed deep learning system. It is also noted that CARRA specifically only have a 30 hour lead time, which limits the desired "up to 3 day" lead time desired for the developed deep learning system.

With regards to model development, a major development in AROME Arctic in terms of temperature representation over sea ice occurred 10 Oct 2018 (AROME Arctic Changelog, Last Access 21 Jan 2023), in the form of a *snow on ice* variable. As this change is expected to have changed the distribution of 2-meter temperature significantly, especially over sea ice covered grid cells (Batrak et al., 2018; Batrak and Müller, 2019), it has been opted to only consider near surface temperature data from AROME Arctic from 2019 and onwards. This decision is made to avoid having a shift in temperature distribution present in the data, which would exert a negative impact on training the deep learning model.

Though the different datasets in Table (1) have been chosen with the intention to serve as independent products without any intra coupling, it is noted that the sea ice observations used to compute the sea ice concentration trend (Tonboe et al., 2017) is also used to force AROME Arctic with sea ice concentration at the initial timestep (Müller et al., 2017). it is suboptimal to provide input parameters derived from other input parameters, as their correlation may render one of the input parameters obsolete in terms of additional information the deep learning system will infer from the "redundant" predictor. Nonetheless, it is assumed that the impact of the sea ice concentration forcing is low when combined with other surface forcings during the assimilation process. Furthermore, as the sea ice concentration is kept constant at all timesteps (Müller et al., 2017), the correlation between sea ice concentration and atmospheric variables can be assumed to be decaying with time. Thus, both products will be used as input variables, and their overlap is assumed to tend toward zero.

1.3.2 NeXtSIM

The neXt generation Sea Ice Model (neXtSIM) is developed by the Nansen Environmental and Remote Sensing Center and performs the physical simulations for the neXtSIM-F deterministic forecasting platform (Williams et al., 2021). NeXtSIM-F assimilates sea ice concentration from operational OSI SAF sea ice concentration products (Tonboe et al., 2017; Lavelle et al., 2016) and forces the model with oceanic and atmospheric forecasts. Furthermore, the neXtSIM-F platform is not a coupled system, i.e. the neXtSIM sea ice model is not coupled to either and atmospheric or oceanic model. The version of neXtSIM-F data used for this thesis is supplied on a 3km polar stereographic grid on a pan-arctic domain.

NeXtSIM differentiates itself from comparative physical sea ice models as it does not apply a rheology based on the Viscous-Plastic scheme. The rheology of a sea ice model refers to how the model relates ice deformation and ice thickness with the internal stresses in the ice (Hibler, 1979). Instead, NeXtSIM applies a brittle sea ice rheology, specifically the brittle Bingham-Maxwell (BBM) rheology which treats the sea ice as a brittle material rather than a viscous fluid (Ólason et al., 2022). Due to the implementation of the BMM rheology, neXtSIM-F is the first sea ice forecasting system not to use a viscous-plastic scheme (Williams et al., 2021).

With a forecast range of 7 days, data from neXtSIM-F will be used to validate the deep learning system against current high resolution operational sea ice forecasts by serving as a comparable product. NeXtSIM-F is the highest resolution model distributed as part of the Copernicus Marine Environmental Monitoring Service (European Union-Copernicus Marine Service, 2020).

1.3.3 Barents-2.5

Barents-2.5, (hereby Barents) is an operational coupled ocean and sea ice forecasting model under development at MET Norway (Röhrs et al., 2022). The model has been in operation since September 2021. Barents poses the same resolution and projection as AA, i.e. Lambert Conformal Conic with a 2.5km resolution (Röhrs et al., 2022; Müller et al., 2017). Furthermore, Barents also forecasts with a lead time of up to 66 hours, which is the same as AROME Arctic. Since Barents covers the same spatial domain as the deep learning system and forecast with a lead time close to three days, its predicted sea ice concentration will be used for validation purposes.

The sea ice model used in Barents is the Los Alamos sea ice model (CICE) version 5.1, which uses an Elastic Viscous Plastic sea ice Rheology (Hunke et al., 2015). Thus, the CICE model represents sea ice as a viscous fluid which creeps slowly given small stresses and deforms plastically under large stress. It is also noted that the elastic behavior was introduced to benefit the numerical aspects of the model, and can be considered unrealistic from a physical point of view (Hunke and Dukowicz, 1997).

Barents includes an Ensemble Prediction System with 6 members executed for each of the four model runs situated at (00, 06, 12 and 18) (Röhrs et al., 2022). As part of its forcing routine, Barents performs non-homogenous atmospheric forcing of its ensemble members, with one member of each ensemble being forced with AA while the rest of the members are forced using atmospheric data from ECMWF. As such, the members forced with AA seem to perform best with regards to ocean currents, but the atmospheric forcing's impact on SIC performance is unknown at the time of writing (Johannes Röhrs, 2022, pers. commun.). However, there is generally little spread within one ensemble with

regards to sea ice (Röhrs et al., 2022).

The data assimilation scheme applied for Barents is a Deterministic Ensemble Kalman filter, which solves for the analysis with a background error covariance matrix estimated as the variance of the ensemble of background members (Röhrs et al., 2022). Furthermore, it has been expressed by the developers of Barents that the model performance was unsatisfactory up until May / June 2022 due to spin up time of the data assimilation system (Johannes Röhrs, 2022, pers. commun.). As such, forecasts initiated prior to May 2022 will not be assessed for validation purposes due to the expected shift in performance as expressed by the model developers.

Similarly to the neXtSIM-F data in Section (1.3.2), Barents will also be used to validate the deep learning system. However, the forecast range of Barents is only 66 hours, which cuts it short of producing three full daily means. Furthermore, due to the ensemble setup of Barents, it is possible to present a forecast both through the ensemble mean as well as a pseudo deterministic run (single member). However, a forecast from a single Barents member would still be influenced by the other ensemble members during the assimilation stage.

ECMWF IFS is used to force both neXtSIM and Barents with atmospheric variables, whereas the ocean model TOPAZ (Sakov et al., 2012) is used to force neXtSIM (Williams et al., 2021) while only nudging the boundaries of Barents (Röhrs et al., 2022). However, their differences in terms of ensemble setup, model coupling, sea ice rheology as well as domain coverage has led to both products being included for validation of the deep learning system. Moreover, both physical products are of a spatial and temporal scale for operational relevancy (Wagner et al., 2020), similar to the deep learning system.

References

Batrak, Y. and Müller, M.: On the warm bias in atmospheric reanalyses induced by the missing snow over Arctic sea-ice, Nature Communications, 10, https://doi.org/10.1038/s41467-019-11975-3, 2019.

Batrak, Y., Kourzeneva, E., and Homleid, M.: Implementation of a simple thermodynamic sea ice scheme, SICE version 1.0-38h1, within the ALADIN–HIRLAM numerical weather prediction system version 38h1, Geoscientific Model Development, 11, 3347–3368, https://doi.org/10.5194/gmd-11-3347-2018, 2018.

Bauer, P., Beljaars, A., Ahlgrimm, M., Bechtold, P., Bidlot, J.-R., Bonavita, M., Bozzo, A., Forbes, R., Hólm, E., Leutbecher, M., Lopez, P., Magnusson, L., Prates, F., Rodwell, M., Sandu, I., Untch, A., and Vitart, F.: Model Cycle 38r2: Components and Performance, https://doi.org/10.21957/XC1R0LJ6L, 2013.

Dette avsnittet ble kjelkete, men ønsker å si noe om at det er mer relevant å sammenlikne mot disse to modellene, og ikke typ en klimamodell for havis,

Cavalieri, D. J. and Parkinson, C. L.: Arctic sea ice variability and trends, 1979–2010, The Cryosphere, 6, 881–889, https://doi.org/10.5194/tc-6-881-2012, 2012.

Comiso, J. C., Cavalieri, D. J., Parkinson, C. L., and Gloersen, P.: Passive microwave algorithms for sea ice concentration: A comparison of two techniques, Remote Sensing of Environment, 60, 357–384, https://doi.org/10.1016/s0034-4257(96)00220-9, 1997.

Dee, D. P., Uppala, S. M., Simmons, A. J., Berrisford, P., Poli, P., Kobayashi, S., Andrae, U., Balmaseda, M. A., Balsamo, G., Bauer, P., Bechtold, P., Beljaars, A. C. M., van de Berg, L., Bidlot, J., Bormann, N., Delsol, C., Dragani, R., Fuentes, M., Geer, A. J., Haimberger, L., Healy, S. B., Hersbach, H., Hólm, E. V., Isaksen, L., Kållberg, P., Köhler, M., Matricardi, M., McNally, A. P., Monge-Sanz, B. M., Morcrette, J.-J., Park, B.-K., Peubey, C., de Rosnay, P., Tavolato, C., Thépaut, J.-N., and Vitart, F.: The ERA-Interim reanalysis: configuration and performance of the data assimilation system, Quarterly Journal of the Royal Meteorological Society, 137, 553–597, https://doi.org/https://doi.org/10.1002/qj.828, URL https://rmets.onlinelibrary.wiley.com/doi/abs/10.1002/qj.828, 2011.

Dinessen, F., Hackett, B., and Kreiner, M. B.: Product User Manual For Regional High Resolution Sea Ice Charts Svalbard and Greenland Region, Tech. rep., Norwegian Meteorological Institute, 2020.

European Union-Copernicus Marine Service: Arctic Ocean Sea Ice Analysis and Forecast, https://doi.org/10.48670/MOI-00004, 2020.

Goessling, H. F., Tietsche, S., Day, J. J., Hawkins, E., and Jung, T.: Predictability of the Arctic sea ice edge, Geophysical Research Letters, 43, 1642–1650, https://doi.org/10.1002/2015gl067232, 2016.

Haiden, T., Janousek, M., Vitart, F., Ben-Bouallegue, Z., Ferranti, L., Prates, F., and Richardson, D.: Evaluation of ECMWF forecasts, including the 2021 upgrade, https://doi.org/10.21957/XQNU5O3P, 2022.

Hibler, W. D.: A Dynamic Thermodynamic Sea Ice Model, Journal of Physical Oceanography, 9, 815–846, https://doi.org/10.1175/1520-0485(1979)009<0815:adtsim>2.0.co;2, 1979.

Holland, P. R. and Kimura, N.: Observed Concentration Budgets of Arctic and Antarctic Sea Ice, Journal of Climate, 29, 5241–5249, https://doi.org/10.1175/jcli-d-16-0121.1, 2016.

Hunke, E. C. and Dukowicz, J. K.: An Elastic–Viscous–Plastic Model for Sea Ice Dynamics, Journal of Physical Oceanography, 27, 1849–1867, https://doi.org/10.1175/1520-0485(1997)027<1849:aevpmf>2.0.co;2, 1997.

Hunke, E. C., Lipscomb, W. H., Turner, A. K., Jeffery, N., and Elliott, S.: CICE: the Los Alamos Sea Ice Model Documentation and Software User's Manual Version 5.1 LA-CC-06-012, techreport, Los Alamos National Laboratory, Los Alamos NM 87545, 2015.

Kern, S., Lavergne, T., Notz, D., Pedersen, L. T., Tonboe, R. T., Saldo, R., and Sørensen,

A. M.: Satellite passive microwave sea-ice concentration data set intercomparison: closed ice and ship-based observations, The Cryosphere, 13, 3261–3307, https://doi.org/10.5194/tc-13-3261-2019, 2019.

Kern, S., Lavergne, T., Notz, D., Pedersen, L. T., and Tonboe, R.: Satellite passive microwave sea-ice concentration data set inter-comparison for Arctic summer conditions, The Cryosphere, 14, 2469–2493, https://doi.org/10.5194/tc-14-2469-2020, 2020.

Køltzow, M., Schyberg, H., Støylen, E., and Yang, X.: Value of the Copernicus Arctic Regional Reanalysis (CARRA) in representing near-surface temperature and wind speed in the north-east European Arctic, Polar Research, 41, https://doi.org/10.33265/polar.v41.8002, 2022.

Lavelle, J., Tonboe, R., Tian, T., Pfeiffer, R.-H., and Howe, E.: Product User Manual for the OSI SAF AMSR-2 Global Sea Ice Concentration Product OSI-408, Tech. Rep. 1.1, Danish Meteorological Institute, 2016.

Lavelle, J., Tonboe, R., Jensen, M. B., and Howe, E.: Validation Report for OSI SAF Global Sea Ice Concentration Product OSI-401-b, Tech. Rep. 1.2, Danish Meteorological Institute, 2017.

Lavergne, T., Sørensen, A. M., Kern, S., Tonboe, R., Notz, D., Aaboe, S., Bell, L., Dybkjær, G., Eastwood, S., Gabarro, C., Heygster, G., Killie, M. A., Brandt Kreiner, M., Lavelle, J., Saldo, R., Sandven, S., and Pedersen, L. T.: Version 2 of the EUMETSAT OSI SAF and ESA CCI sea-ice concentration climate data records, The Cryosphere, 13, 49–78, https://doi.org/10.5194/tc-13-49-2019, URL https://tc.copernicus.org/articles/13/49/2019/, 2019a.

Lavergne, T., Tonboe, R., Lavelle, J., and Eastwood, S.: Algorithm Theoretical Basis Document for the OSI SAF Global Sea Ice Concentration Climate Data Record OSI-450, OSI-430-b, techreport 1.2, 2019b.

Melsheimer, C.: ASI Version 5 Sea Ice Concentration User Guide, Tech. rep., Institute of Environmental Physics, University of Bremen, 2019.

Melsom, A., Palerme, C., and Müller, M.: Validation metrics for ice edge position forecasts, Ocean Science, 15, 615–630, https://doi.org/10.5194/os-15-615-2019, 2019.

Müller, M., Batrak, Y., Kristiansen, J., Køltzow, M. A. Ø., Noer, G., and Korosov, A.: Characteristics of a Convective-Scale Weather Forecasting System for the European Arctic, Monthly Weather Review, 145, 4771–4787, https://doi.org/10.1175/mwr-d-17-0194.1, 2017.

Ólason, E., Boutin, G., Korosov, A., Rampal, P., Williams, T., Kimmritz, M., Dansereau, V., and Samaké, A.: A New Brittle Rheology and Numerical Framework for Large-Scale Sea-Ice Models, Journal of Advances in Modeling Earth Systems, 14, https://doi.org/10.1029/2021ms002685, 2022.

Palerme, C., Müller, M., and Melsom, A.: An Intercomparison of Verification Scores for Evaluating the Sea Ice Edge Position in Seasonal Forecasts, Geophysical Research Letters, 46, 4757–4763, https://doi.org/10.1029/2019gl082482, 2019.

Ronneberger, O., Fischer, P., and Brox, T.: U-Net: Convolutional Networks for Biomedical Image Segmentation, in: Lecture Notes in Computer Science, pp. 234–241, Springer International Publishing, https://doi.org/10.1007/978-3-319-24574-4_28, 2015.

Röhrs, J., Gusdal, Y., Rikardsen, E., Moro, M. D., Brændshøi, J., Kristensen, N. M., Fritzner, S., Wang, K., Sperrevik, A. K., Idžanović, M., Lavergne, T., Debernard, J., and Christensen, K. H.: "in prep for GMD" An operational data-assimilative coupled ocean and sea ice ensembleprediction model for the Barents Sea and Svalbard, p. 20, 2022.

Sakov, P., Counillon, F., Bertino, L., Lisæter, K. A., Oke, P. R., and Korablev, A.: TOPAZ4: an ocean-sea ice data assimilation system for the North Atlantic and Arctic, Ocean Science, 8, 633–656, https://doi.org/10.5194/os-8-633-2012, 2012.

Smith, D. M.: Extraction of winter total sea-ice concentration in the Greenland and Barents Seas from SSM/I data, International Journal of Remote Sensing, 17, 2625–2646, https://doi.org/10.1080/01431169608949096, 1996.

Spreen, G., Kaleschke, L., and Heygster, G.: Sea ice remote sensing using AMSR-E 89-GHz channels, Journal of Geophysical Research, 113, https://doi.org/10.1029/2005jc003384, 2008.

Spreen, G., Kwok, R., and Menemenlis, D.: Trends in Arctic sea ice drift and role of wind forcing: 1992-2009, Geophysical Research Letters, 38, n/a–n/a, https://doi.org/10.1029/2011gl048970, 2011.

Sørensen, A. M., Lavergne, T., and Eastwood, S.: Global Sea Ice Concentration Climate Data Record Product Uses Manual Product OSI-450 & OSI-430-b, Tech. Rep. 2.1, Norwegian Meteorological Institute, 2021.

Tonboe, R., Lavelle, J., Pfeiffer, R.-H., and Howe, E.: Product User Manual for OSI SAF Global Sea Ice Concentration, Tech. Rep. 1.6, Danish Meteorological Institute, 2017.

Wagner, P. M., Hughes, N., Bourbonnais, P., Stroeve, J., Rabenstein, L., Bhatt, U., Little, J., Wiggins, H., and Fleming, A.: Sea-ice information and forecast needs for industry maritime stakeholders, Polar Geography, 43, 160–187, https://doi.org/10.1080/1088937x.2020.1766592, 2020.

Williams, T., Korosov, A., Rampal, P., and Ólason, E.: Presentation and evaluation of the Arctic sea ice forecasting system neXtSIM-F, The Cryosphere, 15, 3207–3227, https://doi.org/10.5194/tc-15-3207-2021, 2021.

Yu, X., Rinke, A., Dorn, W., Spreen, G., Lüpkes, C., Sumata, H., and Gryanik, V. M.: Evaluation of Arctic sea ice drift and its dependency on near-surface wind and sea ice conditions in the coupled regional climate model HIRHAM–NAOSIM, The Cryosphere, 14, 1727–1746, https://doi.org/10.5194/tc-14-1727-2020, 2020.

Zampieri, L., Goessling, H. F., and Jung, T.: Predictability of Antarctic Sea Ice Edge on Subseasonal Time Scales, Geophysical Research Letters, 46, 9719–9727, https://doi.org/10.1029/2019gl084096, 2019.